ELSEVIER

Ceramics International 27 (2001) 29–37

CERAMICS INTERNATIONAL

www.elsevier.com/locate/ceramint

Sintering behaviour of pressed red mud wastes from zinc hydrometallurgy

L. Montanaro [a,*], N. Bianchini [a], J.Ma. Rincon [b], M. Romero [b]

[a] *Department of Materials Science and Chemical Engineering, Politecnico, Corso Duca degli Abruzzi, 24, 10129 Turin, Italy*
[b] *The Glass-Ceramics Laboratory, Instituto E. Torroja de Ciencias de la Costrucción, CSIC, Serrano Galvache, s/n 28033 Madrid, Spain*

Received 3 February 2000; received in revised form 23 February 2000; accepted 20 March 2000

Abstract

The sinterability of two different ceramic wastes coming from the hydrometallurgy processing of zinc ores was investigated in view of their low-cost reuse as porous building materials for heat and sound insulation. Their chemical composition, the phase and mass changes during heat treatment were firstly investigated for setting up the thermal cycle for their densification. The materials demonstrated to sinter to high final density without any sintering aid at temperatures close to 1300°C. Their sintering behaviour was strongly dependent on their composition and particularly on the amount and type of impurities, leading to the formation of a transitory liquid phases which assist the densification of the main crystalline phases, hematite and magnetite or zinc ferrite, as a function of the process used for iron separation. Many of the heavy metal oxides are part of low-soluble crystalline phases or of the glassy phase yielded at the higher temperatures: this behaviour could contribute to reduce the environmental impact of these materials dependent to the heavy metal leaching.

Keywords: A. Sintering; B. Impurities; B. Microstructure-final; B. X-ray methods

1. Introduction

In hydrometallurgy processing of zinc ores, sulphuric acid is the reagent used for leaching and decomposition of ores, concentrates or roasted calcine. Iron is always present in the raw materials as an impurity and has to be removed from the leach solution. At present, about 75% of the world's zinc is produced hydrometallurgically, mainly by acid leaching of roasted zinc sulphur concentrated. The iron is usually precipitated from acid leach solutions as jarosite or goethite. In jarosite process a basic ferric sulphate is precipitated at 95°C and pH = 1.5. The general formula of jarosite is $X[Fe_3(SO_4)_2(OH)_6]$, where X is a cation such as Na^+, K^+, NH_4^+, Ag^+, 1/2 Pb^{2+} or H_3O^+. In goethite (FeOOH) process the iron is precipitated at 90°C and pH = 2–3.5 [1]. Both processes leave large amounts of residues, which are toxic due to concentration of heavy metals (i.e. zinc and lead). The production of this type of wastes in the European Union is evaluated in 600,000 ton/year. To avoid leaching of the residues, they are stored in closed containers or in sealed reservoirs, which is a costly and environmentally unsatisfactory procedure [1].

Recent papers have reported on the use of different methods to recycle jarosite and goethite wastes, such as inertization by vitrification [2–5] or even their use as building materials, catalysts, pigments, or refractories.

Though previous work has been carried out in order to sinter original glasses designed from calcined jarosite wastes [6], at present, no attempt has been made to determine the sintering behaviour of jarosite and goethite wastes such as original red muds, even if this characterisation is fundamental in view of their low-cost reuse, for example as building materials. This paper deals with the physical and microstructural characterisation during sintering in the temperature range of 900–1300°C of such as received jarosite and goethite wastes. This research represents the first step in the frame of a work focused on the recycling of these wastes for the production of porous building materials to be proposed as heat and sound insulators.

* Corresponding author. Tel.: +39-11-564-4680; fax: +39-11-564-4665.

E-mail addresses: negro@athena.polito.it (L. Montanaro), jrincon@fresno.csic.es (J.Ma. Rincon).

0272-8842/01/$20.00
PII: S0272-8842(00)00038-9

2. Materials and methods

Jarosite-process [supplied by Asturiana del Zinc (Spain)] and goethite-process [supplied by Nuova Samin (Italy)] wastes are labelled as A and B, respectively, from now on. Both wastes were low-temperature (105°C) dried powders. These wastes were characterised by means of chemical analysis (X-ray fluorescence, FRX, and inductively coupled plasma with atomic emission spectroscopy, ICP-AES), X-ray diffraction, XRD (Philips PW1710 diffractometer using CuK_α radiation), particle size analysis (Malvern Particle Sizer 3600D using absolute ethanol as dispersion medium), simultaneous thermal analysis [thermogravimetry (TG) and differential thermal analysis (DTA), Netzsch STA 409, using Pt crucibles with calcined alumina as reference in static air, heating rate of 5°C/min].

Compacts were obtained by uniaxial compression of the waste powders under 50 MPa. Green densities of 2.56 and 2.16 g/cm^3 were reached for the wastes A and B, respectively. The sintering behaviour was investigated by dilatometric measurements on the green bodies up to 1300°C with an isothermal step of 30 minutes (Netzsch Dilatometer 402E, heating and cooling rate of 5°C/min).

The residual open porosity and the mean pore size of bodies sintered at 900, 1000, 1150, 1200 and 1300°C (temperatures chosen on the ground of the above dilatometric curves) for 30 min were determined by Hg porosimetry (Carlo Erba Porosimeter 2000).

The microstructural and mineralogical evolution during sintering were investigate by means of scanning electron microscopy (SEM, Hitachi S-2300) on polished and thermally etched samples and XRD respectively. Scanning electron microscopy (Jeol JSM-840) coupled with an energy-dispersive X-ray analysis (EDX) spectroscopy [Kevex Si (Li) with Be window detector and Rontec spectrometer with software programme with ZAF corrections marketed as Edwin name] was used to examine the microstructure and composition of original powders and sintered specimens. The EDX average analysis have been carried out in specimens without metal coating and spot and small areas microanalysis were obtained after coating with a thin layer (approximately 20 nm) of gold evaporated in vacuum in an Emscope sputtering equipment.

3. Results and discussion

The particle size distributions of the powders, as-received and after ultrasonic treatment to destroy soft agglomerates, are given in Fig. 1. Waste A showed a narrower particle size distribution, located below 20 μm with a mean size of about 4 μm. On the contrary, for waste B the curve ranged from 1 to 70 μm with a mean size of about 17 μm. After the ultrasonic treatment only a slight change was observed in waste A (the mean size decreased to about 3 μm), while a more significant variation was shown in waste B, with a final mean size of 11 μm.

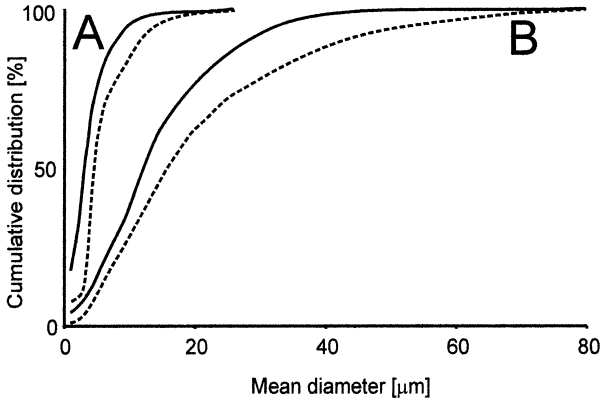

Fig. 1. Particle size distribution of the wastes A and B, before (dotted line) and after (solid line) ultrasonic treatment.

Fig. 2 shows the XRD patterns of the as-received wastes. Ammonium iron sulfate hydroxide [$NH_4Fe_3(SO_4)_2(OH)_6$, ammoniojarosite, JCPDS file 26-1014] was the main phase detected in the dried waste A, while waste B contained zinc ferrite ($ZnFe_2O_4$), quartz, an hydrate lead iron phosphate ($PbFe(PO_4)_2(OH,H_2O)_6$), anglesite ($PbSO_4$), and some other phases containing sulphur ($CaSO_4{\cdot}2H_2O$ and FeS). Dried waste B, even if otained from the goethite-process as declared by the Supplier, did not contain FeO(OH).

The DTA–TG curves of the as-received jarosite and goethite wastes are given in Fig. 3. Sample A showed two weight loss steps, both associated to an endothermic effect. The first weight loss was imputed to the dehydration and decomposition of the ammoniojarosite, while the second peak could be associated to the decomposition of lead sulfate as supported by the XRD patterns obtained after calcination (see below). The total weight loss of dried A up to 1200°C was more than 45%. Waste B presented two endothermic peaks at low temperature (105–150°C), associated to gypsum decomposition, an exothermic peak at 580°C, due to hematite formation, and an endothermic effect at 760°C once again imputed to metal sulfates decomposition on the ground of the XRD data. Its total weight loss up to 1200°C was 27%.

The chemical analyses were performed on the wastes calcined at 1200°C till to constant weight (Table 1) and they are in agreement with previous data on similar materials [4,5]. The major components of waste A are Fe_2O_3 and ZnO (more than 84% in total) and a significant alkaline oxide content (Na_2O+K_2O) is also present. Waste B contains a lower Fe_2O_3 content: the weight ratio between iron and zinc oxides decreases from 10.7 in waste A to 3.9 in waste B.

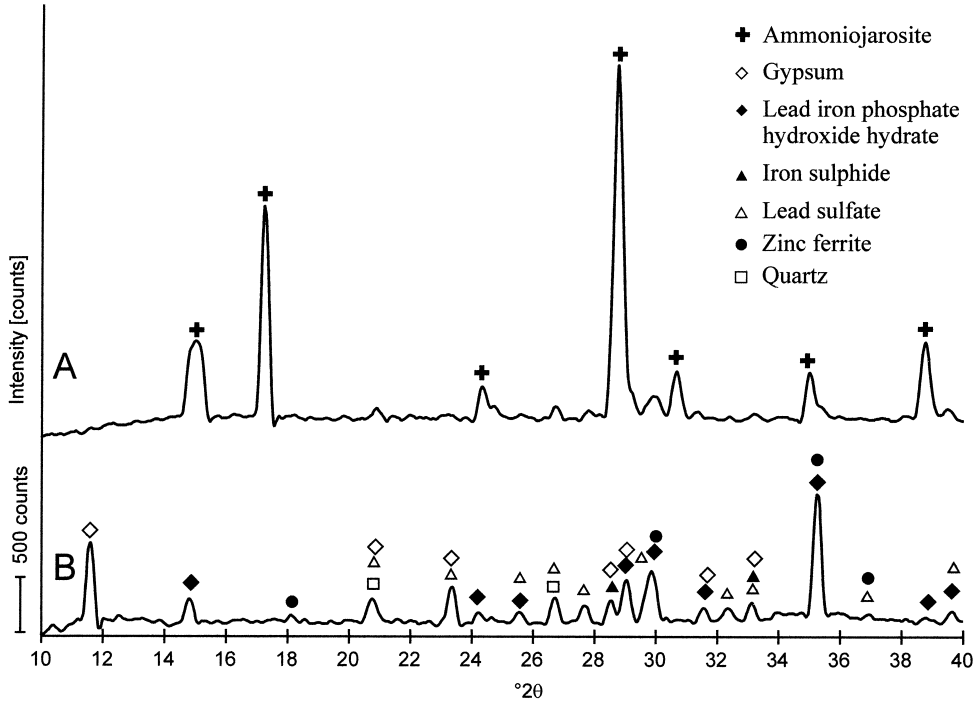

Fig. 2. X-ray diffraction patterns of the dried wastes A and B.

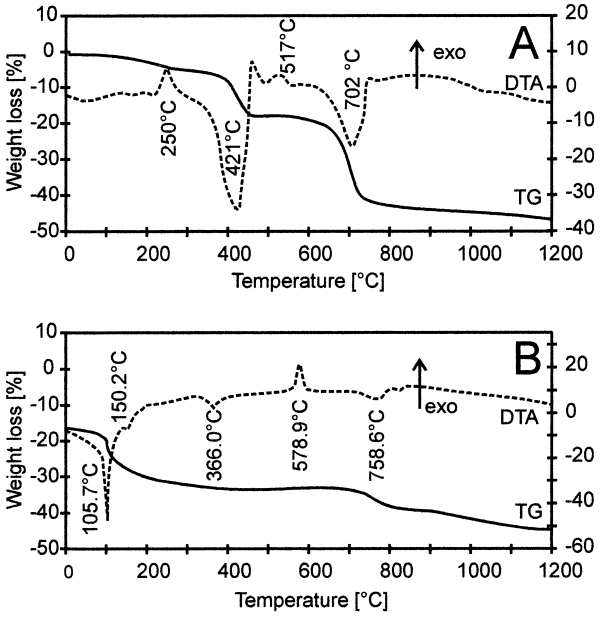

Fig. 3. DTA–TG curves of the dried wastes A and B.

Fig. 4 shows the XRD patterns of the waste A treated at different temperatures in the range 200 to 1300°C. After the decomposition of the ammoniojarosite, at 650°C hematite, quartz, anglesite ($PbSO_4$) were clearly detected. Magnetite (Fe_3O_4) also appeared at 900°C, whereas the lead sulfate was progressively substituted by lead oxide sulfate ($PbO{\cdot}PbSO_4$). Hematite and magnetite remained the only phases detected after heat

Table 1
Mean chemical components of wastes A and B expresses as oxides

Oxide	A (wt.%)	B (wt.%)
Fe_2O_3	77.4	67.9
ZnO	7.24	17.6
SiO_2	4.5	3.85
Al_2O_3	0.28	0.9
CaO	0.08	1.3
$Na_2O + K_2O$	4.01	0.15
$PbO + SO_2$	6.49	8.3

treatment at 1300°C. The evolution in the waste B as a function of the temperature is presented in Fig. 5. No significant changes in the peak intensities and phases were observed after treatment in the range 200°C to 650°C, except the decomposition of the lead iron phosphate hydroxide hydrate. At 650°C, FeS disappeared and $FeSO_4$ and Fe_2O_3 were formed. At 900°C some peaks of anhydrite ($CaSO_4$) were detected also thanks to the reduction of the total peak number: lead and iron sulfate completely disappeared and lower amounts of quartz were detected. Zinc ferrite was the only phase clearly evidenced after thermal treatment at 1300°C. This result is consistent with the compositional data reported in Table 1. In the case of waste A, the molar ratio between Fe_2O_3 and ZnO is more than 5:1, whereas in the case of waste B it is 2:1, justifying the prevalence of the zinc ferrite (Fe_2O_3/ZnO molar ratio of 1:1) in this latter.

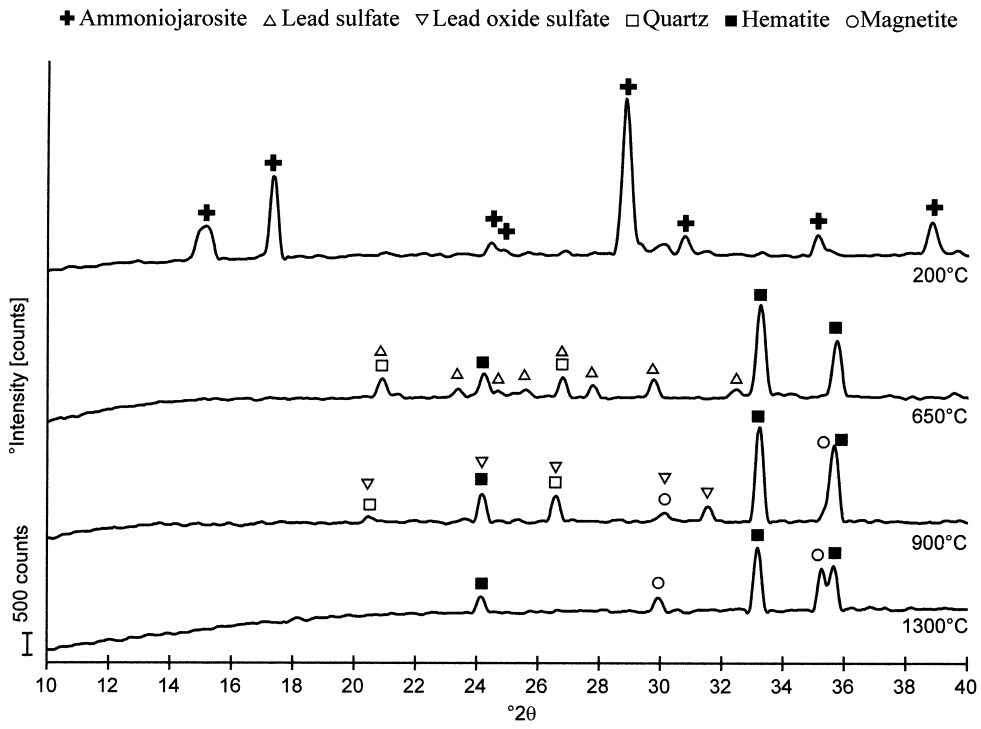

Fig. 4. X-ray diffraction patterns of the waste A treated at different temperatures.

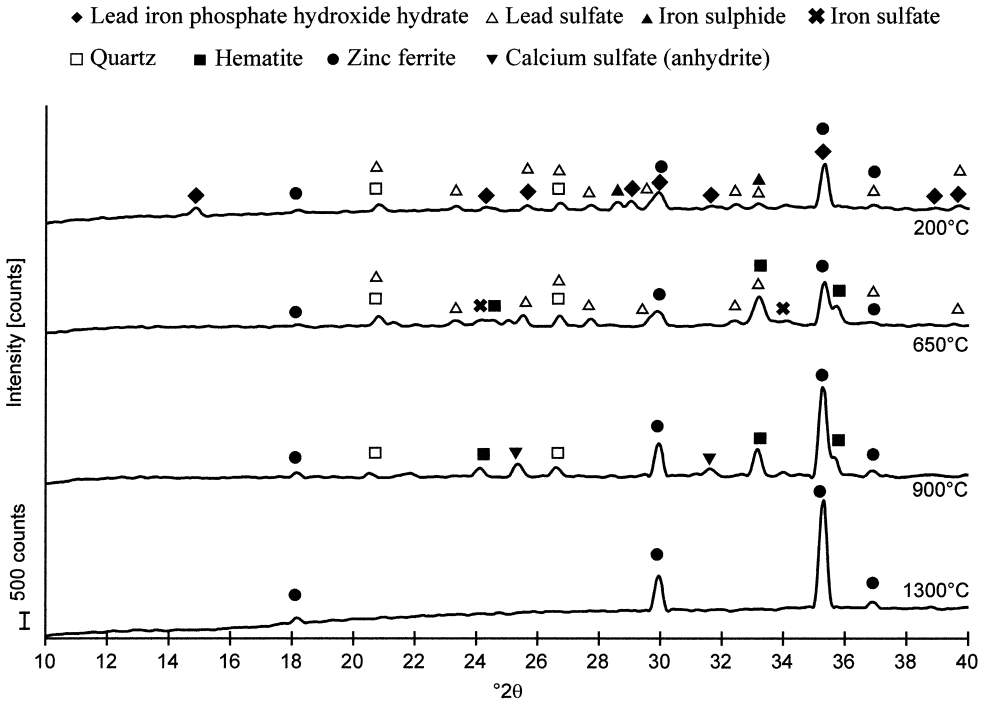

Fig. 5. X-ray diffraction patterns of the waste B treated at different temperatures.

Considering the chemical and mineralogical compositions of the wastes and the data reported in the literature on the sintering behaviour of materials based on Fe_2O_3 [7–10] or $ZnFe_2O_4$ [11–14], a final sintering temperature of 1300°C was chosen to characterise their sinterability. To limit the significant shrinkage at low temperature due to the phase transformations and associated weight loss (see the above XRD and DTA-TG data), the two powders were pre-treated at 650°C for 1 h.

The dilatometric curves of the wastes are given in Fig. 6. The shrinkage of waste A started at about 860°C and consisted of two steps: the first one finished at about 1120°C and the second one started at 1200°C and continued in the isothermal step. A single shrinkage step starting at 870°C was observed in the dilatometric curve of waste B. The final shrinkage was 24 and 31% and the final density was 4.55 and 4.33 g/cm^3 for wastes A and B, respectively. The difference in the final densities can be imputed to the different green density, particle size distribution and chemical composition of the wastes.

Geometrical measurements of the green and sintered bodies put in evidence an anisotropic densification. The samples shrank more in the axial direction (parallel to the measurement bar), whereas a lower shrinkage was observed in the radial directions, which shows a mean shrinkage of 17 and 22.5% for wastes A and B, respectively.

This behaviour can be due to a viscous sintering in presence of a liquid phase; the viscous flow, in fact, seems to be increased under the low pressure imposed by the dilatometer holder.

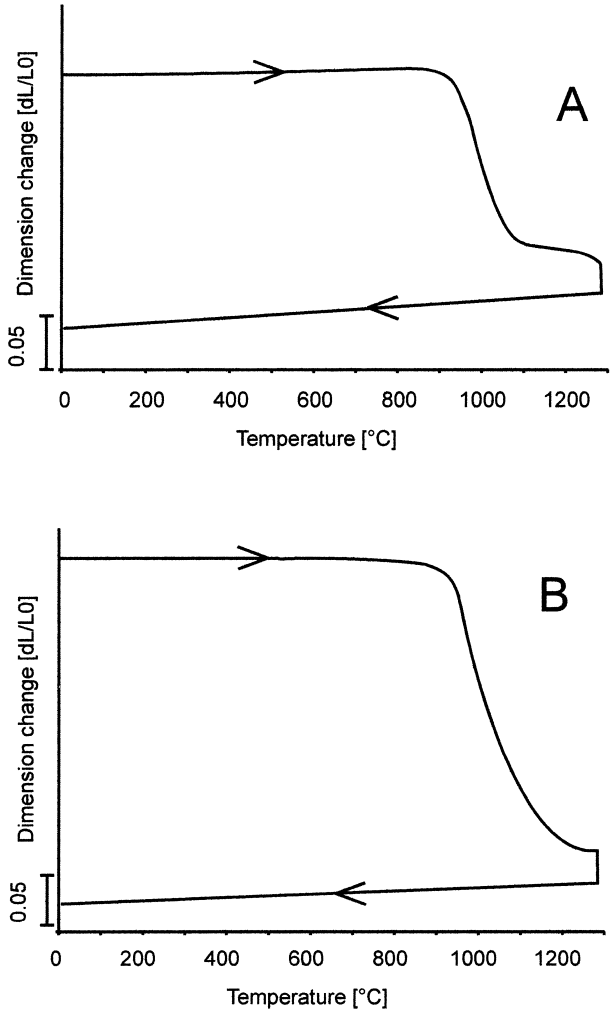

Fig. 6. Dilatometric curves of the wastes A and B pre-treated at 650°C and sintered up to 1300°C (heating and cooling rate of 5°C/min; soaking time at the maximum temperature of 30 min).

The presence of SiO_2, PbO, CaO and alkali oxides in the wastes (Table 1) can be responsible of the formation of small amounts of a liquid transitory phase and it is consistent with the onset shrinkage temperature (~860°C) for both materials [15]. Comparing the XRD patterns after calcination at different temperatures (Figs. 4 and 5) it can be easily observed that quartz and $PbSO_4$ peaks almost completely disappeared in the wastes treated at 900°C. The differences in the shrinkage slope and temperature range can be reasonably imputed to the difference in composition of these liquid phases, as reported in the following EDX data.

Another validation of the hypothesis of liquid phase formation comes from the shrinkage measurements on powder compacts sintered without any pressure. In this case a more homogeneous shrinkage was observed (a mean value of 18.6% for waste A and 24.7% for waste B, being the shrinkage independent from the measurement direction).

Table 2 collects the total open porosity of the sintered wastes after treatment at different temperatures. From these data the first shrinkage step in waste A is the responsible of the quasi-total sintering of the material. At 1150°C, almost all the open porosity was eliminated. On the contrary, a more regular decrease of the open porosity was observed in waste B as a function of temperature and this material was still affected by about 7% of open porosity after sintering at 1300°C.

Fig. 7 shows the evolution of the pore size distribution as a function of the sintering temperatures. Waste A depicts a typical sintering behaviour [16], with smaller pores disappearance and the permanence of very few, large pores having a mean radius of about 4 μm in the final material. In waste B, the incomplete sintering is also evidenced by the final pore distribution: some smaller pores of about 0.02 μm in radius are still present near the bigger pores having a mean size of about 3 μm.

By SEM–EDX analyses performed on sintered samples their microstructural and compositional evolution as a function of temperature was followed (Figs. 8a–d and 9a–d). As shown in the Fig. 8a and b, both materials gave rise to a very heterogeneous microstructure at 1150°C. Crystal shape and distribution changed significantly from a region to another and the presence of a

Table 2
Total open porosity in the sintered bodies as a function of temperature

Sintering temperature (°C)	A (% porosity)	B (% porosity)
900	35.0	50.2
1000	6.0	32.4
1150	0.9	17.2
1200	0.9	9.9
1300	0.8	7.3

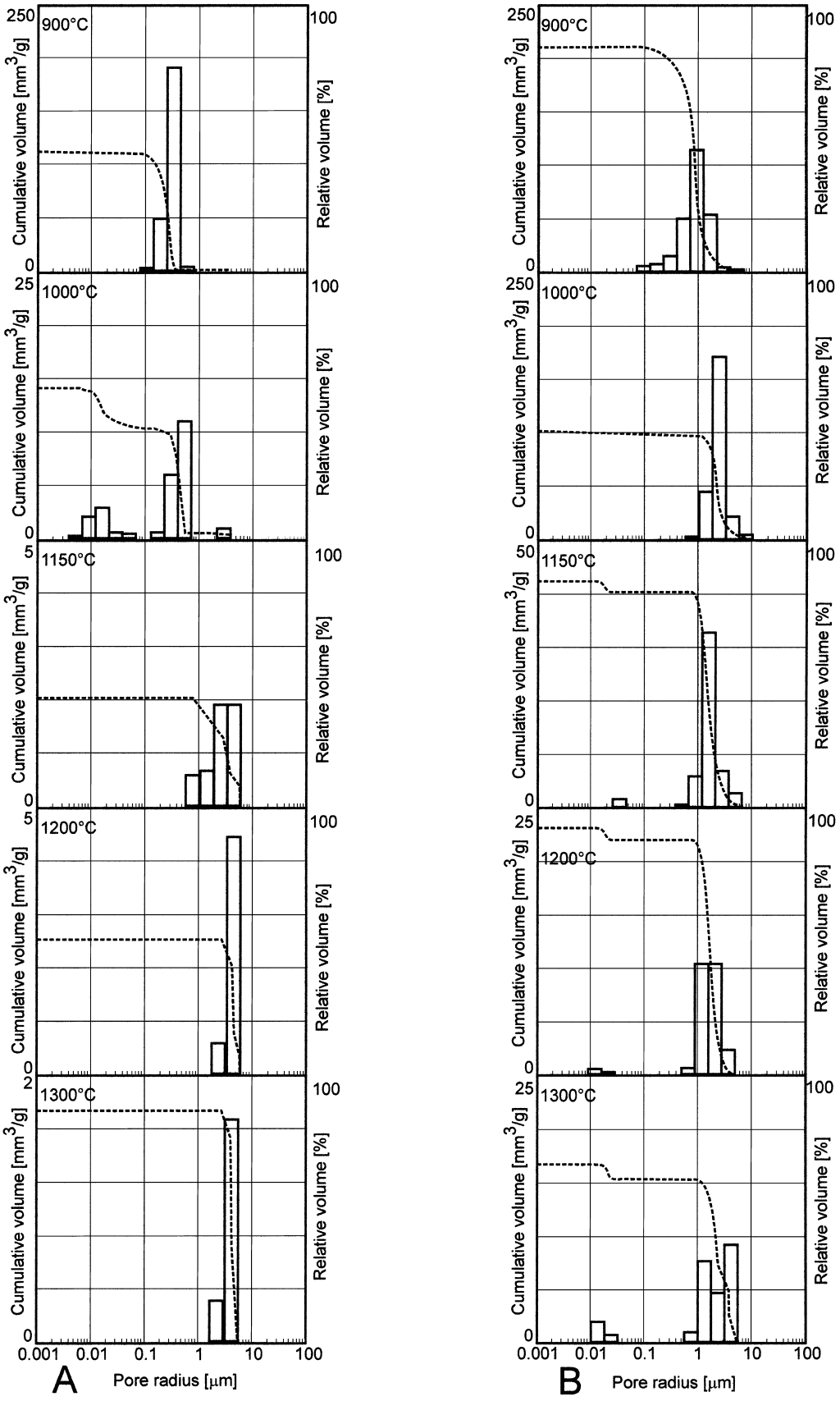

Fig. 7. Evolution of the pore size distribution as a function of the sintering temperature of the wastes A and B.

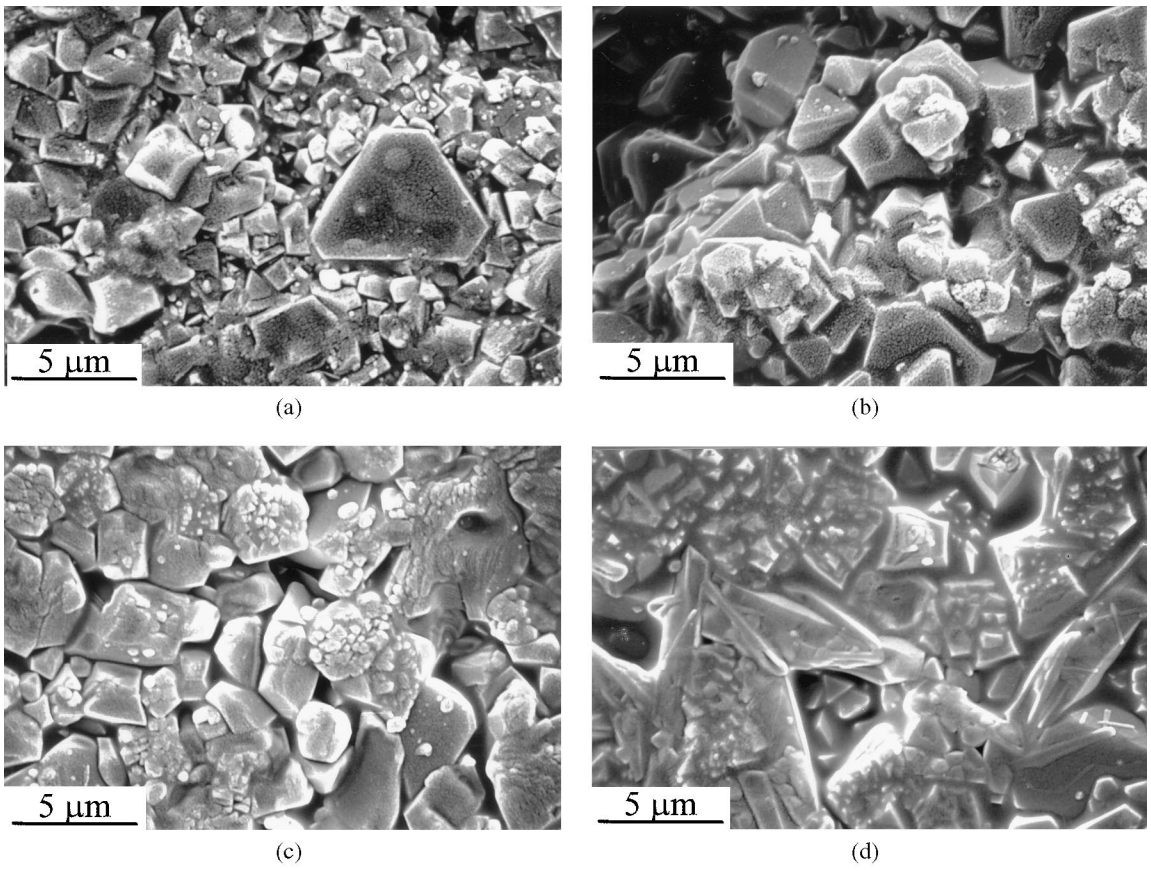

Fig. 8. Scanning electron micrographs of the sintered materials: (a) waste A at 1150°C; (b) waste B at 1150°C; (c) waste A at 1200°C; (d) waste B at 1200°C.

glassy phase surrounding the crystals was not clearly evidenced. At a higher temperature (1200°C, Fig. 8c and d) the microstructure looked more homogeneous in sample A, still heterogeneous in B. In both cases small crystallites of hematite precipitated near pyramidal zinc ferrite crystals, as confirmed by EDX analyses. However, the relative amount of these two phases significantly changed from sample A to B. In addition, in sample B large glassy phase regions were observed near elongated zinc ferrite crystals, while glassy phase was more homogeneously distributed and less evident in sample A.

At the higher sintering temperature (1300°C) (Fig. 9) both wastes depicted the presence of a glassy phase surrounding the crystals. The volume fraction of the glassy phase seems to be higher in the sintered sample B and many glassy pockets can be easily observed. After sintering at 1300°C waste A showed a more homogeneous microstructure in terms of crystal shape and size and it is formed by equiaxially shaped well-facetted grains, having a size ranging between 1 and 5 μm. According to the XRD data these were hematite and magnetite crystals.

Waste B presented a more heterogeneous microstructure with the appearance of a few elongated grains near equiaxial ones, larger grains (of about 5 μm) near smaller ones (less than 1 μm). Many small grains were preferentially located near or inside the glassy pockets, suggesting a partial recrystallisation from the amorphous phase. Most of the grain boundaries were roundish, and only few facetted surfaces were observed. According to XRD data the sample was mainly made of zinc ferrite crystals.

The SEM observations were also in agreement with the porosimetry measurement: a very low porosity volume fraction was observed on the fracture surface of waste A, whereas a more porous surface was presented by sample B.

Due to the heterogeneity of the sintered materials, semi-quantitative EDX analyses have been only performed on the denser materials with well-developed microstructures, that is on pellets A treated between 1150 and 1300°C and on pellets B heated at 1300°C, in order to understand more in detail the phases composition and the influence of the liquid phase on sintering. Firstly, average area analyses were performed on the materials obtained at the different sintering temperatures. This type of analysis, even if not comparable to the chemical analysis shown in Table 1, allowed to analytically distinguish the different phases present in the microstructure due to large deviations from the average composition. Definitive assessment cannot be

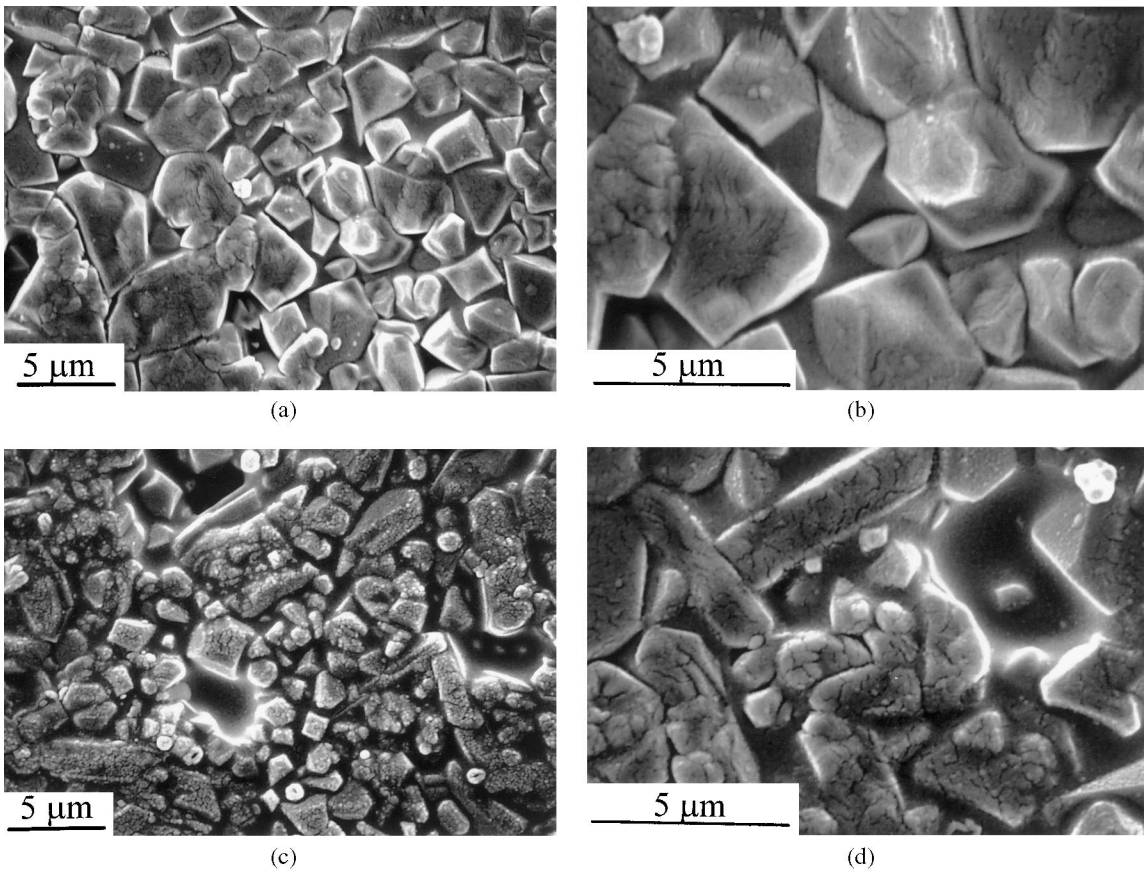

Fig. 9. Scanning electron micrographs micrographs of the sintered materials at 1300°C: (a and b) waste A; (b and c) waste B.

obtained due to the heterogeneity of the structure and composition; however, some trends and clear indications can be drawn out. For an easy comparison of results, the compositions are frequently expressed as metal oxides weight percentages.

For sample A an easier description of the data can be performed considering the evolution of the phase composition starting from the higher temperature. At 1300°C (Table 3) some pyramidal zinc ferrite grains were detected near iron oxide particles. The mean composition of the zinc ferrite, performed on many grains, demonstrated that significant percentages of CuO (4–6 wt.%) were entrapped in $ZnFe_2O_4$ crystals and this could be favourable in reducing leaching of these two heavy metals. Therefore, CuO can be considered vicariant of ZnO to warrant the correct Fe_2O_3/MO molar ratio.

Analysing the composition of many glassy pockets, it is possible to underline that the alkali oxides (0.9–1.5 wt.%) and CaO (4–6 wt.%) contents are quite constant whereas a high variability of PbO (25–40 wt.%) was evidenced. The mean composition of these glassy pockets and their mean SiO_2/Al_2O_3 weight percent ratio are reported in Table 4. This ratio increased from about 3.63 at 1300°C to about 3.81 at 1200°C: being alumina a refractory oxide, the lower sintering temperature is

Table 3
Sample A: mean analysis results on pyramidal zinc ferrite crystals after treatment at 1300°C

Compound	Wt.%	Number of moles
Fe_2O_3	67.52	0.423
ZnO	29.92	0.367
CuO	5.56	0.07
Molar ratio $Fe_2O_3/(ZnO+CuO)=0.967$		

Table 4
Sample A: mean composition of the glassy pockets after treatment at 1300 and 1200°C

Compounds	Mean wt.% at 1300°C	Mean wt.% at 1200°C
SiO_2	45.12	39.55
Al_2O_3	12.44	10.36
PbO	33.15	38.14
CaO	5.16	4.31
ZnO	3.02	5.34
Na_2O+K_2O	1.11	1.04
CuO	–	1.14
SiO_2/Al_2O_3	3.63	3.81

Table 5
Sample B: mean composition of the glassy pockets after treatment at 1300°C

Compounds	Mean wt.% at 1300°C
SiO_2	18.59
Al_2O_3	1.85
PbO	39.59
CaO	14.36
ZnO	21.69
$Na_2O + K_2O$	2.25
CuO	1.65
SiO_2/Al_2O_3	10.04

consistent with an increase of the relative amount of silica in the glassy phase. In addition, at the lower considered temperature the relative percentage of PbO is higher, ranging from about 36 to 44 wt.%; this datum could support the hypothesis that the very first liquid phase formed during sintering was mostly yielded by the reaction of quartz and lead oxide. In fact, the silica/alumina weight ratio at 1150°C grew at a value of about 4 and the relative lead oxide content in the glassy phase increased too: a mean weight percentage of 57.4 was detected. At this temperature zinc ferrite grains with vicariant CuO are already present, but in a very limited number than at the higher temperatures, whereas ZnO and CuO contents are more significant in the glassy phase, reaching values of about 7 and 3 wt.% respectively. These data support the hypothesis that zinc and copper oxides preferentially reacted with iron oxide to yield zinc ferrite in the high temperature range.

Also in sample B, CuO was vicariant of ZnO in zinc ferrite crystals, even if lower amount of this oxide (about 2 wt.%) were detected in the grains. The mean composition of the glassy pockets after treatment at 1300°C is reported in Table 5. This glass presented higher amounts of zinc and calcium oxides but lower of silica and alumina than the glassy phase in A. Its silica/alumina weight ratio ranged from 8 to about 13.5. The high microstructural heterogeneity and porosity did not enable to perform reliable measurements on this material sintered at lower temperatures.

4. Conclusions

The study performed on the as-received red mud wastes, made of jarosite and goethite, has demonstrated that these materials are able to sinter to high final density without additions, at temperatures close to 1300°C. Their sinterability comes from the presence of impurities, such as SiO_2, PbO, CaO and alkaline oxides, leading to the formation of a transitory liquid phase which assist the densification of the main crystalline phases, hematite, magnetite and/or zinc ferrite. Many experimental evidences of the formation of this transitory liquid phase, mainly given by the reaction of quartz and lead sulfate, were reported.

In this sense, this process can be considered as an "intrinsic liquid phase sintering" (ILPS), which is of special interest, making less costly the processing and sintering of the industrial wastes.

In addition, the formation of this glassy phase entrapping large amounts of heavy metals could be positive in recycling these materials as well as their high sinterability is promising in their use for developing porous or cellular structures. For supporting this hypothesis some leaching tests of the densified materials as obtained in this work or as porous materials for heat and sound insulation must be performed.

References

1 M. Romero, J.Ma. Rincon, Microstructural characterisation of a goethite waste from zinc hydrometallurgical process, Mater. Let. 31 (1997) 67–73.
2 M. Pelino, C. Cantalini, P.P. Boattini, C. Abbruzzese, J.Ma. Rincon, J.E. Rincon, Glass-ceramic materials obtained by recycling goethite industrial wastes, Resources, Conservation and Recycling 10 (1994) 171–176.
3 M. Romero, J.Ma. Rincon, C. Cantalini, M. Pelino, Properties and applications of high iron content glass-ceramics obtained by recycling of goethite wastes, in: P. Vincenzini (Ed.), Ceramics: Charting the Future, Techna, Faenza, Italy, 1995, pp. 229–236.
4 M. Romero, J. Ma Rincon, Preparation and properties of high iron oxide content glasses obtained from industrial wastes, J. Eur. Ceram. Soc. 18 (1998) 153–160.
5 A. Karamanov, C. Cantalini, M. Pelino, A. Hreglich, Kinetics of phase formation in jarosite glass-ceramics, J. Eur. Ceram. Soc. 19 (1999) 527–533.
6 J.Ma. Rincón, M. Pelino, M. Romero, Glass-ceramics obtained from axial pressing and sintering of vitrified high iron content red muds, in: M. Pelino, G.C. Pellacani (Eds.), Valorisation and Recycling of Industrial Wastes, Mucchi Editore, Modena, 1998, pp. 169–182.
7 C.M. Kramer, R.M. German, Low-temperature sintering of iron oxides, J. Am. Ceram. Soc. 61 (1978) 340–342.
8 T. Yamaguchi, H. Kosha, Sintering of acicular Fe_2O_3 powder, J. Am. Ceram. Soc. 64 (1981) C-84–C-85.
9 T. Yamagushi, H. Kosha, Behavior of pores in the sintering of acicular Fe_2O_3 powder, J. Am. Ceram. Soc. 66 (1983) 210–213.
10 J. Certo, C.S. Furtado, A.R. Ferreira, J.M. Ferdigao, Studies on densification of α-Fe_2O_3 ceramics, J. Mater. Sci. 30 (1995) 3248–3250.
11 N. Yoneda, I. Katoh, Duplex structure formation in oxide magnetic materials, J. Am. Ceram. Soc. 61 (1978) 465.
12 M.N. Rahaman, L.C. De Jonghe, Reaction sintering of zinc ferrite during constant rates of heating, J. Am. Ceram. Soc. 76 (1993) 1739–1744.
13 S. Komarneni, E. Fregeau, E. Breval, R. Roy, Hydrothermal preparation of ultrafine ferrites and their sintering, J. Am. Ceram. Soc. 71 (1988) C-26–C-28.
14 F.J.C.M. Toolenaar, M.T.J. Verhees, Reactive sintering of zinc ferrite, J. Mater. Sci. 23 (1988) 856–861.
15 R.S. Roth, T. Negas, L.P. Cook (Eds.), Phase Diagrams for Ceramists, Vol. 4, Am. Ceram. Soc., Westerville, OH, 1981, pp. 107–109.
16 F.F. Lange, Sinterability of agglomerate powders, J. Am. Ceram. Soc. 67 (1984) 83–89.